Oxidation of benzyl alcohol and carbon monoxide using gold nanoparticles supported on MnO_2 nanowire microspheres

Mosaed Alhumaimess,[a][b] Zhongjie Lin,[a] Qian He,[c] Li Lu,[c] Nickolaos Dimitratos,[a] Nicholas F. Dummer,[a] Marco Conte,[a] Stuart H. Taylor,[a] Jonathan K. Bartley,[a] Christopher J. Kiely[b] and Graham J. Hutchings*[a]

[a] Dr M. Alhumaimess, Dr Z. Lin, Dr N. Dimitratos, Dr N. F. Dummer, Dr M. Conte, Dr S. H. Taylor, Dr J. K. Bartley, Prof G. J. Hutchings

Cardiff Catalysis Institute, School of Chemistry, Cardiff University, Cardiff, CF10 3AT, UK.

Email: Hutch@cardiff.ac.uk

[b] Dr M. Alhumaimess

Department of Chemistry, College of Science, Al Jouf University, PO Box 2014, Sakaka, KSA

[c] Dr Q. He, Mr L. Lu, Prof C. J. Kiely

Department of Materials Science and Engineering, Lehigh University, 5 East Packer Avenue, Bethlehem, Pennsylvania 18015, USA.

Keywords: nanomaterials, heterogeneous catalysis, gold catalysis, CO oxidation, benzyl alcohol oxidation

Table of Contents Entry

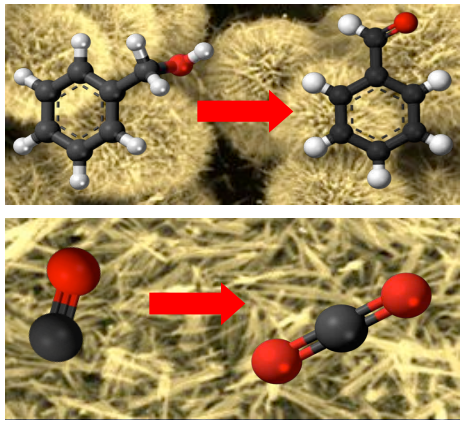

Shape selectivity: Different nanostructured MnO_2 materials were prepared by adjusting the synthesis conditions. When used as a support for gold oxidation catalysts it was found that α–MnO_2 spherical agglomerates performed the best in the liquid phase oxidation of benzyl alcohol, whereas β–MnO_2 nanowires performed better for gas phase CO oxidation.

Abstract

MnO_2 was synthesised as a catalyst support material using a hydrothermal method. This involved reacting $MnSO_4.H_2O$ and $(NH_4)_2S_2O_8$ at 120 °C for a range of crystallisation times, which affords control over the morphology and phase composition of MnO_2 formed. Gold was deposited on these supports using sol-immobilisation, impregnation and deposition precipitation methods and the resultant materials were used for the oxidation of benzyl alcohol and carbon monoxide. The effect of the support morphology on the dispersion of the gold nanoparticles and the consequent effect on the catalytic performance is described and discussed.

Introduction

The selective oxidation of alcohols to their corresponding aldehydes is an important process. Aldehydes are valuable compounds as intermediates in chemical synthesis as well as in the perfumery industry.[1-3] However, the commercial production of aldehydes tends to use oxygen donors, such as chromate or permanganate, that can be expensive and toxic.[4-8] In view of the recent focus on atom efficiency and environmental impact, it would be highly desirable to find alternative methods to oxidize the alcohol moiety. One alternative approach is to use a catalyst in the presence of oxygen under solvent-free reaction conditions. In this respect the oxidation of alcohols to aldehydes represents a demanding target reaction.

There has been considerable interest in using supported gold nanoparticles as oxidation catalysts. Gold was for many years considered to be an unreactive metal for catalysis. However, studies involving carbon monoxide oxidation and acetylene hydrochlorination[9,10] have shown that supported gold nanoparticles can be highly effective catalysts. Subsequently, nanoparticulate gold catalysts have attracted significant attention due to their distinctive catalytic properties. Gold catalysts have been reported to perform well for many chemical reactions such as CO oxidation,[9] direct synthesis of hydrogen peroxide from oxygen and hydrogen,[11-14] the water gas shift reaction,[15] epoxidation of olefins,[16,17] selective oxidation of alcohols[8,18-20] and total oxidation of hydrocarbons.[21] The catalytic performance of gold catalysts essentially relies on the size of the constituent gold particles. Nevertheless, there are other factors that can inherently affect the catalyst activity such as gold oxidation state, the synthesis method and the choice of support. With supported gold catalysts, the structure and the morphology of the support can play a major role in the catalyst performance.[22] The support morphology can influence the catalyst activity as it can affect parameters such as the gold particle size,[23-26] the metal-support interaction,[24-29] the exposure of more reactive planes that are rich in oxygen,[30-32] and the dispersion and reducibility of gold catalysts.[33-35] Recently, we illustrated that

gold is more active for the solvent-free oxidation of benzyl alcohol when supported on ceria foam due to the facile reduction of its surface compared to more conventionally synthesised ceria.[36]

In this work, MnO_2 was synthesised hydrothermally according to the method of Yang et al.[37] which involves the oxidation of hydrated manganese sulfate $MnSO_4.H_2O$ with ammonium persulfate $(NH_4)_2S_2O_8$ at 120 °C. In a related study Subramanian et al.[38] reacted aqueous solutions of $MnSO_4.H_2O$ with $KMnO_4$ at 140 °C and found that the morphology changed from plate-like to nano rods as the hydrothermal treatment time was increased. We have now applied this logic to the method of Yang et al. and synthesised a series of MnO_2 materials, which have subsequently been evaluated as a support for Au nanoparticles. Furthermore the catalytic activity of these materials was investigated for the solvent-free oxidation of benzyl alcohol and gas phase CO oxidation.

Experimental Section

Synthesis of MnO_2: MnO_2 supports were synthesised according to the method of Yang et al.[37] Hydrated manganese sulfate $MnSO_4.H_2O$ (14.198 g, Aldrich) was dissolved in water (165 mL) with stirring at room temperature for 15 min. Ammonium persulfate $(NH_4)_2S_2O_8$ (19.169 g, Aldrich) was added with stirring to form a clear solution which was then placed in a sealed autoclave (Baskerville, 250 mL) and heated to 120 °C for a range of times (6-240 h). Following the reaction the resultant black material was recovered by filtration, washed with water (1 L) and dried (60 °C, 24 h). The resultant MnO_2 materials were denoted MnO_2-*x*h, where *x* is the crystallisation time in hours.

Synthesis of the gold sol and the supported gold catalysts: Gold nanoparticles were supported on the MnO_2 materials (1%Au/MnO_2) using the following methods.

(i) Sol-immobilisation method (SI): A 1 wt.% solution of PVA (Aldrich, MW = 10 000, 80% hydrolysed) was added to an aqueous $HAuCl_4$ solution (0.062 M, equivalent to 10 mg of Au) with vigorous stirring (PVA/Au (w/w) = 1.2). A 0.1 M freshly synthesised solution of $NaBH_4$ ($NaBH_4$/Au

(mol/mol) = 5) was then added to form a red Au sol. After 30 min of sol generation, the colloid was immobilized by adding MnO_2 (0.99g) (acidified to pH 1 using sulfuric acid) under vigorous stirring. After 2 h the slurry was filtered, washed thoroughly with distilled water and dried (110 °C,16 h). All sol-immobilised catalysts were subsequently water treated according to the method of Lopez-Sanchez et al.[39] Typically, the catalyst (0.4 g) was placed in a round bottom flask and water (100 mL) was added into the flask. This flask was connected to a reflux condenser and placed in an oil bath which was heated at 90 °C for 1 h. The slurry was filtered and washed thoroughly with distilled water (800 mL) and dried (110 °C, 16 h).

(ii) Impregnation method (IM): An aqueous solution of $HAuCl_4.3H_2O$ (0.062 M, equivalent to 10 mg of Au) was added to MnO_2 (0.99 g) with stirring. The resultant paste was dried (110 °C, 16 h) and calcined in static air at 400 °C for 3 h.

(iii) Deposition precipitation (DP): 0.99 g MnO_2 was mixed with 150 ml distilled water and stirred at 60 °C. A solution of $HAuCl_4.3H_2O$ (0.062 M, equivalent to 10 mg of Au) was added, followed by the drop-wise addition of NaOH solution to maintain an overall pH of 9. After 1.5 h the solution was filtered and washed with 1 L distilled water. The catalyst was dried (110 ºC, 16 h) and calcined in static air at 400 °C for 3h.

Oxidation of benzyl alcohol: Benzyl alcohol oxidation reactions were carried out in a glass Colaver reaction vessel (50 mL) at a constant pressure of oxygen (1 barg unless otherwise stated). Typically, the vessel was charged with benzyl alcohol (2 g) and catalyst (Au/MnO_2, 20 mg, unless otherwise stated). The vessel was then purged 5 times with oxygen. The vessel was then heated to 120 °C under stirring for 4 h. Analysis of the products was carried out using a GC (Varian Star 3400 CX with a 30 m CP-Wax 52 CB column) equipped with an FID. Quantification was carried out using mesitylene as a standard and the products were identified by comparison with commercially obtained pure samples.

Oxidation of carbon monoxide: Catalyst samples were evaluated for CO oxidation using a fixed-bed laboratory microreactor operated at atmospheric pressure. Typically CO (5000 ppm in synthetic air) was fed to the reactor at a controlled rate of 20-40 mL/min using mass flow controllers and passed over the catalyst (25-100 mg). The catalyst temperature was maintained at 30 °C by immersing the quartz bed in a thermostatically controlled water bath. The products were analysed using online gas chromatography (Varian 3800 with a 1.5 m packed carbosieve column) equipped with a TCD. The space-time yield ($g_{CO2}/kg_{CAT}/h$) was calculated from the CO conversion after 140 min time online.

Catalyst characterization: Powder X-ray diffraction (XRD) was performed using a PANalytical X'Pert Pro diffractometer fitted with an X'Celerator detector using a CuK_{α} X-ray source operated at 40 kV and 40 mA. Surface area was determined by nitrogen adsorption at -196 °C using a Micromeritics Gemini 2360 according to the Brunauer-Emmett-Teller (BET) method. All samples were degassed under N_2 for 2 h at 110 °C prior to analysis**.** TPR analysis was performed on a Quantachrome ChemBET instrument. Samples (0.02 g) were pre-treated at 100 °C (ramp rate = 20 °C min^{-1}) under He for 1 h prior to reaction to clean the surface. Analysis was performed under 10 % H_2/Ar (BOC 99.99%, 25 ml min^{-1}) from 30-850 °C (ramp rate = 20 °C min^{-1}). Scanning electron microscopy (SEM) analyses were carried out using a Carl Zeiss EVO-40 microscope equipped with a backscatter detector and an Oxford Instruments Si_{Li} energy dispersive X-ray detector. The powder samples were sprinkled sparsely over carbon tape mounted on an aluminium stub before sputter coating with gold for *ca.* 5 min prior to the SEM analysis. TEM images were obtained using a 200kV JEOL 2000FX electron microscope equipped with a thermionic LaB_6 source. The samples were ground in high purity ethanol and a drop of the suspension was placed on a holey carbon film supported on a 300 mesh copper TEM grid. Laser Raman spectroscopy was used for analysing the amount of PVA that remained on the sol-immobilised materials before and after the water treatment method using a Renishaw inVia Ramascope equipped with an 785 nm laser.

Results and discussion

Synthesis of MnO_2 and Au/MnO_2: A set of MnO_2 materials were synthesised according to the method of Yang *et al.*[37] with different crystallization times ranging from 6 h to 240 h. X-ray diffraction showed that although all materials were comprised of crystalline MnO_2, two different phases were present (Fig. 1). For MnO_2 samples crystallised for 6-24 h, the major phase present was α-MnO_2 with a small amount of the γ-phase.[37,40] However, when the crystallization time was increased above 24 h, β-MnO_2[40] was predominantly formed and this remained stable for all of the longer crystallization times investigated (72-240 h). The morphology of the MnO_2 samples changed significantly with the crystallization time (Fig. 2). For 6 to 12 h crystallization times the thin MnO_2 crystallites were ordered into spherical structures reminiscent of sea urchins. However, at 24 and 48 h these spheres started to collapse exhibiting cracked shell-like structures which evolved to a needle or nanowire structure at longer crystallization times (72-240 h). The surface areas and average micropore diameters of the materials are shown in Table 1 for all the MnO_2 supports and their corresponding Au/MnO_2 catalysts. It is apparent that the samples obtained after 6 and 12 h crystallization have the highest surface areas. The surface area was found to markedly decrease as the crystallization time increased for both the MnO_2 supports and the Au/MnO_2 catalysts. However, the crystallization time had no discernable effect on the average pore diameter. Furthermore, the surface areas increased significantly after adding Au to the MnO_2-12h and MnO_2-24h, (*i.e.* the spherical agglomerates of nanowires) whereas the addition of Au had no effect on from the surface area of the materials crystallized for >48 h (*i.e.* isolated nanowires). It is apparent from Fig. 3 that adding gold had no observable effect on the support morphology and the SI Au/MnO_2 catalysts.

Oxidation of benzyl alcohol using Au/MnO_2: The effect of the catalyst synthesis method (IM, SI and DP) on benzyl alcohol oxidation was initially investigated using MnO_2-12h as the support. It is apparent from Table 2 that under the same conditions, the materials synthesised using the SI method

demonstrated the best catalytic performance for the oxidation of benzyl alcohol whereas the IM method catalysts had a very poor performance. Therefore, SI was adopted as the preferred method of synthesis for catalysts used in further detailed testing studies involving benzyl alcohol oxidation.

The results of the oxidation of benzyl alcohol using all the bare MnO_2 support morphologies and their corresponding Au catalysts synthesised by SI, together with those treated with water are presented in Table 3. The MnO_2 materials without Au were found to be quite active for this reaction, and generally their activity increased as the crystallisation time increased. In particular the α-MnO_2 polymorph synthesised for 6-24 h that has a microsphere agglomerate structure showed lower activity than the more isolated β-MnO_2 needles synthesised for 48-240 h. However, upon Au addition, the activity of those catalysts that have the microsphere agglomerate structure was more active, and it is apparent that the activity trend was now reversed with the catalytic activity decreasing as the synthesis time of the underlying MnO_2 support material increased. For example, the conversion decreased from 8.8 % for the 1% Au/MnO_2-12h catalyst to 5.4 % for the 1% Au/MnO_2-240 h catalyst.

Two representative catalyst samples, namely the SI Au/MnO_2-12h (microsphere agglomerates) and Au/MnO_2-96h (nanowires), that showed different catalytic performance towards benzyl alcohol oxidation were characterised further by TEM imaging in order to investigate the effect of the substrate morphology on the gold particle size (Fig. 4). Although the same Au sol was used as the precursor for all the catalysts, the resultant Au particle size varied significantly in the actual catalysts. For the Au/ MnO_2-12h material, the Au particles were larger (~20 nm) than for the Au/MnO_2-96h (~5 nm). Furthermore, the Au particles were more highly dispersed on the MnO_2-96h material. This suggests that the β-MnO_2 nanowire material is a much more suitable support for Au deposition, due to an enhanced Au-MnO_2 interaction which imparts a greater stability against sintering. It is well known that the morphology of the support can strongly influence the final Au particle size of the catalysts[23-26] and

we recently showed that the same starting Au sol gave larger Au particles when supported on a ceria foam compared to a commercial nanocrystalline ceria.[36]

Surprisingly, the Au/MnO_2-12h sample that exhibited larger Au nanoparticles actually gives a higher activity for the oxidation of benzyl alcohol than the Au/MnO_2-96h material. Catalysis by gold is very dependent on the Au particle size and factors such as the synthesis method, the choice of support[22] and even the support structure/morphology can play a major role in determining the performance.[23-26] Although the origin of this higher activity for the Au/MnO_2-12h catalyst might be attributed to a more optimal combination of Au particle size along with the high surface area of the spherically agglomerated MnO_2 support morphology.

The corresponding catalysts synthesised by the water-treated SI method did not show any improvement in the activity over the SI catalysts. The water treatment was thought to enhance the removal of the PVA that covers the gold nanoparticles. During the benzyl alcohol oxidation the facile removal of PVA ligands from supported gold nanoparticles is achieved by the benzyl alcohol itself, which under reaction conditions acts as an effective solvent for PVA (PVA is soluble in benzyl alcohol at 120 °C). To confirm this postulate, the 1% Au/MnO_2-12h catalyst was treated in water and in benzyl alcohol. The treated catalysts, PVA, the MnO_2 support and a set of PVA-impregnated MnO_2 samples were analysed by laser Raman spectroscopy (Fig. 5a). It is apparent, from expanding the region between 500 and 750 cm^{-1} that the band that appears at 576 cm^{-1} for the support, which is attributed to the Mn-O lattice vibration in MnO_2, is present in both the water-treated catalysts but is absent in the untreated catalyst (Fig 5b). Furthermore, this band is visible for the low concentrations of PVA on MnO_2 but decreases as the concentration of PVA increased (Fig. 5b).

The morphology of the supports also had a slight effect on the product selectivities obtained (Table 3). In general, benzaldehyde was the major product with minor amounts of benzyl benzoate and benzoic

acid for the catalysts with the spherical agglomerate morphology while benzaldehyde was the only product observed in case of the catalysts with the more isolated nanowire structure. All of these products originate from oxidation reactions[41,42] and it should be noted that no toluene or any other non-oxidation products were observed.

The effect of the reaction time on the conversion and selectivity for the SI Au/MnO_2-12h material is shown in Table 4. The conversion increased with the reaction time and only benzaldehyde was observed at the beginning of the reaction. However, a minor amount of benzyl benzoate was produced after 4 h of reaction time. This indicates that the partial oxidation of benzyl alcohol is stable at shorter reaction times. However, after an additional 4 h, subsequent oxidation of benzaldehyde occurred which is in-line with our previous observation of the possible origin of the by-products formed during benzyl alcohol oxidation.[43]

The reusability characteristics of the SI Au/MnO_2-12h catalyst was also investigated (Table 5). Following the standard reaction carried out for a 4 h time period the catalyst was recovered by centrifugation followed by one of two different treatment procedures. In the first procedure, the centrifuged catalyst was washed with solvent (20 ml, ethanol or acetone) and then dried (110 °C, 1 h). In the second method, the centrifuged catalyst was dried (110 °C, 1 h) without a washing step. The solvent used to wash the centrifuged catalyst prior to drying was found to have a significant effect. When ethanol was used there was a marked decrease in conversion. Washing with acetone improved the reusability of the recovered catalyst but the conversion still decreased markedly compared to the fresh catalyst. However, when no solvent treatment was used, there was a significant enhancement in the catalyst activity as compared to the solvent treated catalyst with 100 % selectivity to benzaldehyde in all reuse experiments. Electron microscopy comparisons of the catalyst morphology before and after use confirmed that the structures are stable under these conditions (Fig. 7).

Oxidation of carbon monoxide using Au/MnO_2: Having tested the catalysts for a liquid phase reaction the catalysts were then investigated in the gas phase for carbon monoxide oxidation. Initially, the Au/MnO_2-12h catalyst was synthesised using four methods (IM, SI, water-treated SI and DP). Figure 8 shows that under the same reaction conditions, the DP and water-treated SI materials were best for CO oxidation. It is clear that the IM method exhibited a very poor performance in comparison with the other methods. Therefore, the DP and SI (with and without water-treatment) catalysts were selected for more in-depth CO oxidation analysis. Table 6 and Supplemental Figures S1 and S2 show that the activity of the materials derived via the DP synthesis route was found to be slightly better than the water-treated SI method while both of them displayed much higher activity than the untreated SI materials.

The SI catalysts were firstly tested using 100 mg of the catalyst, a 20 ml/min flow rate at a reaction temperature of 30 ºC. The results in Table 6 show that they were not very active and the best catalyst achieved less than 35 % conversion with a space-time yield (STY) of <3 $g_{CO2}/kg_{CAT}/h$. However, following the water washing treatment[39] these SI catalysts became very active for CO oxidation under the same conditions. Water-treated 1% Au sol-immobilised on MnO_2 synthesised that has been crystallised for 48, 72, 96, 120 and 240 h all showed 100 % conversion. Hence, the flow rate was doubled to 40 ml/min (Fig. S1b) in order to determine the relative activities of the catalysts. However, the Au/MnO_2-72, Au/MnO_2-96 and Au/MnO_2-120 catalysts still showed 100 % conversion and it was only when the amount of the catalyst was decreased to 50 mg that it became apparent that the water treated 1% Au/MnO_2-96h was the best catalyst for CO oxidation with a STY of 15.5 $g_{CO2}/kg_{CAT}/h$. The increased activity of the water treated catalysts is clearly due to improved reactant accessibility following the removal of the PVA stabilizer from the catalysts.[39]

A similar set of experiments was carried out for the DP series of Au/MnO_2 catalysts (Table 6 and Fig. S2). The DP materials showed comparable trends, albeit with a higher level of catalytic performance, compared to the water treated SI catalysts. From Table 6 it is clear that 1% Au/MnO_2-96h synthesised by DP exhibited optimal performance displaying 100 % CO conversion, even when the flow rate was decreased to 40 ml/min and the catalyst mass limited to 50 mg (90 % conversion for the corresponding catalyst synthesised by the SI method with water treatment). The conversion of the DP catalyst reached~70 % only when the catalyst mass decreased to 25 mg (Fig. S2b). The most active DP derived catalyst gave an impressive STY of 21 $g_{CO2}/kg_{CAT}/h$.

TEM was used to examine the effect of the synthesis method on the Au particle size distribution. Two catalyst samples (*i.e.* Au/MnO_2-96h) that have the same support morphology and phase (β-MnO_2 nanowires) but synthesised by different methods (SI and DP) were characterised by TEM. Representative micrographs of both catalysts and their corresponding Au particle-size distributions are shown in Fig. 9 that confirms that both methods produced small particles and a high dispersion of Au on the supports. It is apparent that Au nanoparticles in both cases have a narrower particle size distribution with mean values of 2.5 nm and 6.9 nm for the DP and SI methods respectively. The larger mean size exhibited by the SI material is a consequence of the initial size of the Au sol before immobilization, whereas the DP material is not affected by such limitations, allowing access to smaller Au particles.

The presence to the protective PVA ligands that are inherent to the SI synthesis method seem to be an important factor in causing the observed activity difference between the untreated SI and DP catalysts. However, the DP catalysts still showed improved activity over the water treated SI materials, presumably due to the smaller mean Au nanoparticles formed using the DP method which are well documented to be essential for CO oxidation.[44,45]

For all the catalysts investigated, regardless of their synthesis method, it was found that the catalyst activity increased as the support crystallisation time increased up to 96 h, but then activity decreased slightly for catalysts synthesized beyond 96 h. (Table 6). Generally, the preferred support for CO oxidation was β-MnO_2 nanowires, which is the converse of the situation for benzyl alcohol oxidation where α-MnO_2 microspheres were preferred (Table 1).

TEM was employed to investigate the effect of the morphology of the support on the size of the Au nanoparticles. The SI catalysts Au/MnO_2-12h (α-MnO_2 microspheres) and Au/MnO_2-96h (β-MnO_2 nanowires) were investigated as well as the corresponding DP equivalents (Figs. 9 & 10). It is apparent that both SI and DP methods produced large Au nanoparticles (Fig. 10) when deposited on the α-MnO_2 microsphere structure (MnO_2-12h) and when deposited on the β-MnO_2 nanowire supports (MnO_2-96h), the Au nanoparticles were much smaller and more homogeneously distributed (Fig. 9). This suggests that the Au/MnO_2 interaction is stronger for the β-MnO_2 nanowires producing a greater stability against sintering and therefore better catalyst activity towards CO oxidation. This result is consistent with previous studies by Haruta et al.[44] and Tana et al.[45] who noted that the CO conversion decreases as the mean size of the Au particles increase. They suggested that the smaller Au particles led to an increased peripheral interface length between the metal and support, providing more effective adsorption of CO on the metal and fast surface reduction with oxygen species provided by the support.

It should also be remembered that the reducibility of the support material is an important factor to consider in CO oxidation. The Au particles can interact with superoxide species to facilitate the oxidation of CO when adsorbed on the metal-support interface. For non-reducible supports (*e.g.* SiO_2, Al_2O_3, MgO) the activity depends mainly on the size of Au particles as the adsorption of O_2 occurs on the gold particles.[46] MnO_2, which is intrinsically reducible, is reported to be active for the CO oxidation at relatively high temperatures (> 120 ^{o} C).[47] For instance, Xu et al. reported that the α- and β- polymorphs of MnO_2 exhibit significantly different reactivities, with α-MnO_2 nanorods and β-MnO_2

nanorods becoming most active at 130 ^{o} C at 170 ^{o} C respectively. Interestingly, if these polymorphs were loaded with silver, the Ag/β-MnO_2 was found to be more active than the Ag/α-MnO_2 analogue.[47] These studies demonstrate that both the morphology and crystal structure of the MnO_2 support plays an important role for this reaction. The higher activity of Ag/β-MnO_2 was attributed to the stronger interaction between Ag and MnO_2 support as demonstrated by TPR analysis.[47] To investigate if a similar effect was operating in the present study, TPR analysis was employed to characterise MnO_2 samples that exhibit different morphologies and polymorphic phases, (α-MnO_2-12h nanowire microspheres and β-MnO_2-96h nanowires) and have different mean Au particle sizes when incorporated into a Au/MnO_2 catalyst (Fig. 11). The α-MnO_2-12h support comprising the microspherical agglomerate of crystallites showed reduction peaks at 380 °C and 530 °C (Fig. 11a). It is considered that the lower temperature event is due to the reduction of MnO_2 to Mn_3O_4, whereas the high-temperature feature can be ascribed to the reduction of Mn_3O_4 to MnO.[47,48] However, the reduction temperature was shifted to a significantly lower value, (*i.e.* 300 °C and 405 °C) upon the addition of gold (Fig. 11b). Similar trends were found for the β-MnO_2-96h material having the more isolated nanowire morphology, but with an even greater propensity for reduction as indicated by the presence of the two strong reduction features at 295 and 440 °C(Fig 11c). The addition of Au to β-MnO_2-96h increased the degree of reduction even further and although the reduction peak at 440 °C was retained, two further reduction features were present at 240 and 315 °C (Fig. 11d). The reduction of MnO_2 exhibiting a high degree of crystallinity occurs via three steps corresponding to the reduction of MnO_2 to Mn_2O_3 (the lowest temperature peak), Mn_2O_3 to Mn_3O_4, and then Mn_3O_4 to MnO (the highest temperature peak).[47] Evidently, the surface of β-MnO_2 nanowires supporting the smaller diameter Au nanoparticles was more easily reduced compared to the microspherical agglomerates of α-MnO_2 needles having larger Au particles. This indicates a stronger interaction between Au and the MnO_2 support is the former case, which decreases the reduction temperature. This result supports previous models that smaller Au particles produce stronger Au-support interactions and result in a

greater total length of interfacial perimeter between Au and the oxide support, which allows for more effective CO adsorption and fast surface reduction with oxygen species that are provided by the support.[44,45]

Conclusions

Polymorphs of MnO_2 with different morphologies were hydrothermally synthesised by reacting $MnSO_4.H_2O$ and $(NH_4)_2S_2O_8$ at 120 °C for a range of crystallisation times. At shorter crystallization times microspherical agglomerates of α-MnO_2 nanowires were formed whereas more isolated β-MnO_2 nanowires were produced at longer crystallization times. Au nanoparticles were supported on these various nanostructured MnO_2 supports using SI, DP and IM methods and were tested for benzyl alcohol oxidation and CO oxidation. For benzyl alcohol oxidation, the SI derived catalysts exhibited the best catalytic performance, compared to the other methods. Furthermore absolute activity of SI catalysts were found to be dependent on the support crystallization time, with those having Au supported on α–MnO_2 nanowires self-organised into microspherical agglomerates being the most active for benzyl alcohol oxidation as opposed to Au supported on more isolated β-MnO_2 nanowires. For CO oxidation, catalysts prepared by the DP method displayed the best activity. These DP derived catalysts were found to be more active than those prepared by the water-treated SI method, with both being more active than those from the untreated SI method. This was predominantly ascribed to the considerably smaller size of Au nanoparticles produced by the DP method. Furthermore, for CO oxidation, the water-treated SI catalysts show an improved performance compared to the untreated SI materials due the removal of the shell of PVA ligands that cover the Au particles. The effect of the morphology and structure of the support on the activity towards CO oxidation was also investigated. It was found for all catalysts, regardless of their synthesis method, that the β-MnO_2 nanowires catalysts were preferred for CO oxidation due to the better stability of small Au nanoparticles. This confirmed an

essential requirement for this reaction, that a stronger Au-MnO_2 interaction gives better performance towards CO oxidation. Furthermore, the surface of the β-MnO_2 nanowire catalyst supports were easily reduced, as confirmed by H_2-TPR, due to the strong Au-MnO_2 interaction facilitating the dual adsorption of CO and the surface reduction with oxygen species provided by the support. In summary ,the best catalysts for the oxidation of benzyl alcohol came from SI preparation methods on supports consisting of microsphere agglomerates of α-MnO_2 needles, whereas for CO oxidation catalysts the DP preparation method was preferred in combination with more isolated nanowires of β-MnO_2.

Acknowledgements

We thank the EPSRC and Al Jouf University (MA) for financial support.

References

[1] R.A. Sheldon, J.K. Kochi, *Metal-catalyzed oxidations of organic compounds, Academic Press*, New York, **1981**.
[2] U.R. Pillai, E. Sahle-Demessie, *Appl. Catal. A* **2003,** *245*, 103-109.
[3] M. Hudlický, *Oxidations in organic chemistry*, ACS, Washington DC, **1990**.
[4] W.P. Griffith, J.M. Joliffe, *Dioxygen Activation and Homogenuous Catalytic Oxidation*, Elsevier, Amsterdam, **1991**.
[5] G. Cainelli, G. Cardillo, *Chromium oxidations in organic chemistry*, Springer, Berlin, **1984**.
[6] D.G. Lee, U.A. Spitzer, *J. Org. Chem.* **1970**, *35*, 3589-3590.
[7] F.M. Menger, C. Lee, *Tetrahedron Lett.* **1981**, *22*, 1655-1656.
[8] N. Dimitratos, J.A. Lopez-Sanchez, D. Morgan, A. Carley, L. Prati, G.J. Hutchings, *Catal. Today* **2007**, *122*, 317-324.
[9] M. Haruta, N. Yamada, T. Kobayashi, S. Iijima, *J. Catal.* **1989**, *115*, 301-309.
[10] G.J. Hutchings, *J. Catal.* **1985**, *96*, 292-295.
[11] P. Landon, P.J. Collier, A.J. Papworth, C.J. Kiely, G.J. Hutchings, *Chem. Commun.* **2002**, 2058-2059.
[12] E.N. Ntainjua, M. Piccinini, S.J. Freakley, J.C. Pritchard, J.K. Edwards, A.F. Carley, G.J. Hutchings, *Green Chem.* **2012**, *14*, 170-181.
[13] J.K. Edwards, E. Ntainjua N, A.F. Carley, A.A. Herzing, C.J. Kiely, G.J. Hutchings, *Angew. Chem. Int. Ed.* **2009**, *48*, 8512-8515.
[14] G. Li, J. Edwards, A.F. Carley, G.J. Hutchings, *Catal. Today* **2007**, *122*, 361-364.
[15] Q. Fu, H. Saltsburg, M. Flytzani-Stephanopoulos, *Science* **2003**, *301*, 935-938.
[16] T. Hayashi, K. Tanaka, M. Haruta, *J. Catal.* **1998**, *178*, 566-575.
[17] S. Bawaked, N.F. Dummer, D. Bethell, D.W. Knight, G.J. Hutchings, *Green Chem.* **2011**, *13*, 127-134.
[18] D.I. Enache, D. Barker, J.K. Edwards, S.H. Taylor, D.W. Knight, A.F. Carley, G.J. Hutchings, *Catal. Today* **2007**, *122*, 407-411.
[19] M. Boronat, A. Corma, F. Illas, J. Radilla, T. Ródenas, M.J. Sabater, *J. Catal.* **2011**, *278*, 50-58.
[20] S. Demirel, P. Kern, M. Lucas, P. Claus, *Catal. Today* **2007**, *122*, 292-300.
[21] B.E. Solsona, T. Garcia, C. Jones, S.H. Taylor, A.F. Carley, G.J. Hutchings, *Appl. Catal. A* **2006**, *312*, 67-76.
[22] J. Huang, W.-L. Dai, K. Fan, *J. Catal.* **2009**, *266*, 228-235.
[23] X. Zhang, H. Wang, B.-Q. Xu, *J. Phys. Chem. B* **2005**, *109*, 9678-9683.
[24] K. Ho, K. Yeung, *Gold Bull.* **2007**, *40*, 15-30.
[25] W. Yan, B. Chen, S.M. Mahurin, V. Schwartz, D.R. Mullins, A.R. Lupini, S.J. Pennycook, S. Dai, S.H. Overbury, *J. Phys. Chem. B* **2005**, *109*, 10676-10685.
[26] W. Yan, B. Chen, S.M. Mahurin, S. Dai, S.H. Overbury, *Chem. Commun.* **2004**, 1918-1919.
[27] S. Carrettin, P. Concepción, A. Corma, J.M. López Nieto, V.F. Puntes, *Angew. Chem. Int. Ed.* **2004**, *43*, 2538-2540.
[28] A. Abad, P. Concepción, A. Corma, H. García, *Angew. Chem. Int. Ed.* **2005**, *44*, 4066-4069.
[29] J. Li, J. Chen, W. Song, J. Liu, W. Shen, *Appl. Catal. A* **2008**, *334*, 321-329.
[30] H.-X. Mai, L.-D. Sun, Y.-W. Zhang, R. Si, W. Feng, H.-P. Zhang, H.-C. Liu, C.-H. Yan, *J. Phys. Chem. B* **2005**, *109*, 24380-24385.
[31] Tana, M. Zhang, J. Li, H. Li, Y. Li, W. Shen, *Catal. Today* **2009**, *148*, 179-183.
[32] R. Si, M. Flytzani-Stephanopoulos, *Angew. Chem. Int. Ed.* **2008**, *47*, 2884-2887.
[33] X.-S. Huang, H. Sun, L.-C. Wang, Y.-M. Liu, K.-N. Fan, Y. Cao, *Appl. Catal. B* **2009**, *90*, 224-232.

[34] V. Idakiev, T. Tabakova, A. Naydenov, Z.Y. Yuan, B.L. Su, *Appl. Catal. B* **2006**, *63*, 178-186.
[35] L.-C. Wang, Y.-M. Liu, M. Chen, Y. Cao, He, K.-N. Fan, *J. Phys. Chem. C* **2008**, *112*, 6981-6987.
[36] M. Alhumaimess, Z. Lin, W. Weng, N. Dimitratos, N.F. Dummer, S.H. Taylor, J.K. Bartley, C.J. Kiely, G.J. Hutchings, *ChemSusChem* **2012**, *5*, 125-131.
[37] J.B. Yang, X.D. Zhou, W.J. James, S.K. Malik, C.S. Wang, *Appl. Phys. Lett.* **2004**, *85*, 3160-3162.
[38] V. Subramanian, H. Zhu, R. Vajtai, P.M. Ajayan, B. Wei, *J. Phys. Chem. B* **2005**, *109*, 20207-20214.
[39] J.A. Lopez-Sanchez, N. Dimitratos, C. Hammond, G.L. Brett, L. Kesavan, S. White, P. Miedziak, R. Tiruvalam, R.L. Jenkins, A.F. Carley, D. Knight, C.J. Kiely, G.J. Hutchings, *Nat. Chem.* **2011**, *3*, 551-556.
[40] S. Liang, F. Teng, G. Bulgan, R. Zong, Y. Zhu, *J. Phys. Chem. C* **2008**, *112*, 5307-5315.
[41] M. Jayamani, C.N. Pillai, Journal of Catalysis **1983**, *82*, 485-488.
[42] J.A. Lopez-Sanchez, N. Dimitratos, P. Miedziak, E. Ntainjua, J.K. Edwards, D. Morgan, A.F. Carley, R. Tiruvalam, C.J. Kiely, G.J. Hutchings, *Phys. Chem. Chem. Phys.* **2008**, *10*, 1921–1930.
[44] M. Haruta, S. Tsubota, T. Kobayashi, H. Kageyama, M.J. Genet, B. Delmon, *J. Catal.* **1993**, *144*, 175-192.
[45] Tana, F. Wang, H. Li, W. Shen, *Catal. Today* **2011**, *175*, 541-545.
[46] F. Moreau, G.C. Bond, *Catal. Today* **2007**, *122*, 215-221.
[47] R. Xu, X. Wang, D. Wang, K. Zhou, Y. Li, *J. Catal.* **2006**, *237*, 426-430.
[48] W. Tian, H. Yang, X. Fan, X. Zhang, *J. Hazard. Mater.* **2011**, *188*, 105-109.

Figure and Table Captions

Table 1 Surface area and average pore size for MnO_2 (support) and 1% Au/MnO_2 (SI catalyst) materials.

Table 2 Oxidation of benzyl alcohol over 1% Au/MnO_2-12h catalysts prepared by different synthesis methods.

Table 3 Oxidation of benzyl alcohol over the entire series of sol-immobilised 1% Au/MnO_2 catalysts.

Table 4 Time online data for benzyl alcohol oxidation over the SI Au/MnO_2-12h catalyst.

Table 5 Catalyst reuse data for benzyl alcohol oxidation over the SI Au/MnO_2-12h material.

Table 6 Comparison of space-time-yield of CO_2 over 1% Au/MnO_2 catalysts used for CO oxidation at 30 °C.

Figure 1 XRD patterns of the various MnO_2 materials produced: (a) MnO_2-6h, (b) MnO_2-12h, (c) MnO_2-24h, (d) MnO_2-48h, (e) MnO_2-72h, (f) MnO_2-96h, (g) MnO_2-120h and (h) MnO_2-240h.

Figure 2 SEM micrographs showing the effect of crystallisation time on the MnO_2 morphology: (a) MnO_2-6h, (b) MnO_2-12h, (c) MnO_2-24h, (d) MnO_2-48h, (e) MnO_2-72h, (f) MnO_2-96h, (g) MnO_2-120h and (h) MnO_2-240h.

Figure 3 SEM micrographs of the Au/MnO_2 catalyst materials prepared by sol immobilisation: (a) 1%Au/MnO_2-6h, (b) = 1%Au/MnO_2-12h, (c) 1%Au/MnO_2-24h, (d) 1%Au/MnO_2-48h, (e) 1%Au/MnO_2-72h, (f) 1%Au/MnO_2-96h, (g) 1%Au/MnO_2-120h, (h) 1%Au/MnO_2-240h.

Figure 4 Bright field TEM micrographs of the SI Au/MnO_2 catalysts: (a, a1) Au/MnO_2-12h, and (b, b1) Au/MnO_2-96h.

Figure 5 Raman spectroscopy analysis of: (a) SI Au/MnO_2 catalysts, and (b) reference materials.

Figure 6 CO oxidation results from un-treated and water or benzyl alcohol treated 1% Au/MnO_2-12h; ■ = un-treated 1% Au/MnO_2-12h, ● = 1% Au/MnO_2-12h treated in water and ▲ = 1% Au/MnO_2-12h, ● = 1% Au/MnO_2-12h treated in benzyl alcohol.

Figure 7 SEM micrographs of bare supports and catalysts prepared by sol-immobilisation: (a) MnO_2-12h, (b) Au/MnO_2-12h (prior to testing), (c) Au/MnO_2-12h (post-testing) and (d) Au/MnO_2-12h (after 3rd reuse).

Figure 8 Oxidation of CO over 1% Au/MnO_2-12h[a] catalysts prepared by different synthesis methods: (■) WSI (STY; 4.3 $g_{CO2}/kg_{CAT}/h$), (▲) DP (STY; 4.4 $g_{CO2}/kg_{CAT}/h$), (●) SI (STY; 1.4 $g_{CO2}/kg_{CAT}/h$), (♦) IM (STY; 0.3 $g_{CO2}/kg_{CAT}/h$). Reaction conditions: CO flow rate 20 ml/min, catalyst 100 mg, 30 °C.

Figure 9 Representative TEM micrographs and the corresponding Au particle size distributions for: (a, a1) SI Au/MnO_2-96h, and (b, b1) DP Au/MnO_2-96h.

Figure 10 Representative TEM micrographs and the corresponding Au particle size distributions for: (a, a1) SI Au/MnO_2-12h, and (b, b1) DP Au/MnO_2-12h. (NB. The latter PSD (b1) was derived from measurements on electron backscatter images acquired in the SEM).

Figure 11 TPR measurements for bare support materials and Au/MnO_2 catalysts prepared using sol immobilization: (a) MnO_2-12h, (b) SI Au/MnO_2-12h, (c) MnO_2-96h and (d) SI Au/MnO_2-96h.

Table 1 Surface area and average pore size for MnO_2 (support-only) and 1% Au/MnO_2 (SI catalyst) materials.

Material	Support			Catalyst		
	Area (m^2/g)	Average pore diameter (Å)	Total pore volume (ml/g)	Area (m^2/g)	Average pore diameter (Å)	Total pore volume (ml/g)
MnO_2-6h	71	33	0.06	72	33	0.06
MnO_2-12h	54	35	0.05	61	33	0.05
MnO_2-24h	41	35	0.04	52	33	0.04
MnO_2-48h	19	34	0.02	18	34	0.02
MnO_2-72h	12	34	0.01	11	34	0.01
MnO_2-96h	11	34	0.01	10	34	0.01
MnO_2-120h	11	34	0.009	10	35	0.009
MnO_2-240h	10	34	0.008	9	35	0.008

Table 2 Oxidation of benzyl alcohol over 1% Au/MnO_2-12h catalyst prepared by different synthesis methods.[a]

Preparation Method	Temp (°C)	Conversion (%)	Selectivity (%)				
			benzyl aldehyde	toluene	benzoic acid	benzyl benzoate	benzene
Sol-immobilization (SI)	80	2.6	100	-	-	-	-
	100	4.3	98.0	-	-	2.0	-
	120	8.8	98.5	-	-	1.5	-
Impregnation (IM)	80	0.5	100	-	-	-	-
	100	1.0	100	-	-	-	-
	120	1.9	99	-	1.0	-	-
Deposition precipitation (DP)	80	2.2	99	-	1.0	-	-
	100	3.9	100	-	-	-	-
	120	7.5	99	-	1.0	-	-

[a] Benzyl alcohol (2 g), Catalyst (20 mg), O_2 1 barg, 4 h.

Table 3 Oxidation of benzyl alcohol over the entire series of sol-immobilised 1% Au/MnO_2 catalysts.[a]

Material	Catalyst	Conversion (%)	Selectivity (%)				
			benzyl aldehyde	toluene	benzoic acid	benzyl benzoate	benzene
MnO_2-6h	MnO_2 (Blank)	2.4	99.5	-	0.5	-	-
	SI1% Au/MnO_2	8.6	99.0	-	-	1.0	-
	WSI 1% Au/MnO_2	8.1	100.0	-	-	-	-
MnO_2-12h	MnO_2 (Blank)	2.5	99.3	-	0.7	-	-
	SI 1% Au/MnO_2	8.8	98.5	-	-	1.5	-
	WSI 1% Au/MnO_2	8.3	99.0	-	-	1.0	-
MnO_2-24h	MnO_2 (Blank)	2.8	100.0	-	-	-	-
	SI 1% Au/MnO_2	8.5	97.5	-	-	2.5	-
	WSI 1% Au/MnO_2	8.4	99.5	-	-	0.5	-
MnO_2-48h	MnO_2 (Blank)	3.0	10	-	-	-	-
	SI 1% Au/MnO_2	8.2	98.0	-	0.7	1.3	-
	WSI 1% Au/MnO_2	7.0	99.7	-	-	0.3	-
MnO_2-72h	MnO_2 (Blank)	5.0	100.0	-	-	-	-
	SI 1% Au/MnO_2	7.0	99.7	-	-	0.2	-
	WSI 1% Au/MnO_2	6.8	99.8	-	-	0.2	-
MnO_2-96h	MnO_2 (Blank)	4.0	100.0	-	-	-	-
	SI 1% Au/MnO_2	5.6	100.0	-	-	-	-
	WSI 1% Au/MnO_2	5.5	100.0	-	-	-	-
MnO_2-120h	MnO_2 (Blank)	3.9	100.0	-	-	-	-
	SI 1% Au/MnO_2	5.5	100.0	-	-	-	-
	WSI 1% Au/MnO_2	5.6	100.0	-	-	-	-
MnO_2-240h	MnO_2 (Blank)	3.75	100.0	-	-	-	-
	SI 1% Au/MnO_2	5.35	100.0	-	-	-	-
	WSI 1% Au/MnO_2	5.4	100.0	-	-	-	-

[a] Benzyl alcohol (2 g), Catalyst (20 mg), O_2 1 barg, 120 °C, 4 h.

Table 4 Time on-line data for benzyl alcohol oxidation over the SI Au/MnO_2-12h catalyst.[a]

Time (h)	Conversion (%)	Selectivity (%)				
		benzyl aldehyde	toluene	benzoic acid	benzyl benzoate	benzene
1	4.1	100	-	-	-	-
2	6.0	100	-	-	-	-
3	7.2	100	-	-	-	-
4	8.8	98.5	-	-	1.5	-

[a] Benzyl alcohol (2 g), Catalyst (20 mg), O_2 1 barg, 120 °C, 4 h.

Table 5 Catalyst reuse data for benzyl alcohol oxidation over SI Au/MnO_2-12h material.[a]

Catalyst test	Washing treatment	Conversion (%)	Selectivity (%)				
			benzyl aldehyde	toluene	benzoic acid	benzyl benzoate	benzene
1st test	Ethanol	8.8	98.5	0.0	0.0	1.50	0.0
1st reuse		3.9	100	0.0	0.0	0.0	0.0
2nd reuse		2.6	100	0.0	0.0	0.0	0.0
3rd reuse		2.3	100	0.0	0.0	0.0	0.0
1st test	Acetone	8.8	98.5	0.0	0.0	1.50	0.0
1st reuse		5.0	100	0.0	0.0	0.0	0.0
2nd reuse		3.5	100	0.0	0.0	0.0	0.0
3rd reuse		3.0	100	0.0	0.0	0.0	0.0
1st test	No washing	8.8	98.5	0.0	0.0	1.50	0.0
1st reuse		8.45	100	0.0	0.0	0.0	0.0
2nd reuse		8.40	100	0.0	0.0	0.0	0.0
3rd reuse		7.9	100	0.0	0.0	0.0	0.0

[a] Benzyl alcohol (2 g), Catalyst (20 mg), O_2 1 barg, 120 °C, 4 h.

Table 6 Comparison of space-time-yield of CO_2 over 1% Au/MnO_2 catalysts used for CO oxidation at 30 °C.

Support	Catalyst preparation method (1% Au/MnO_2)	Catalyst mass (mg)	Flow rate (ml/min)	Conversion[a] (%)	STY ($g_{CO2}/kg_{CAT}/h$)
MnO_2-6h	SI	100	20	10.0	0.9
	WSI			53.3	4.6
12 MnO_2-12h	IM	100	20	3.8	0.3
	SI			16.1	1.4
	WSI			50.4	4.3
	DP			51.2	4.4
MnO_2-24h	SI	100	20	19.0	1.6
	WSI			56.0	4.8
	DP				
MnO_2-48h	SI	100	20	28	2.4
	WSI		40	83.7	7.2
	DP		40	90.7	7.8
MnO_2-72h	SI	100	20	30.7	2.6
	WSI	50	40	62.2	10.7
	DP	50	40	77.4	13.3
MnO_2-96h	SI	100	20	33.4	2.9
	WSI	50	40	90.1	15.5
	DP	25	40	61.1	21.0
MnO_2-120h	SI	100	20	33.7	2.9
	WSI	50	40	41.9	7.2
	DP	50	40	66.6	11.4
MnO_2-240h	SI	100	20	29.0	2.5
	WSI	100	40	91.0	7.8
	DP	50	40	52.9	9.1

[a] conversion after 140 minutes time online.

Figure 1 XRD patterns of the various MnO_2 materials produced: (a) MnO_2-6h, (b) MnO_2-12h, (c) MnO_2-24h, (d) MnO_2-48h, (e) MnO_2-72h, (f) MnO_2-96h, (g) MnO_2-120h and (h) MnO_2-240h.

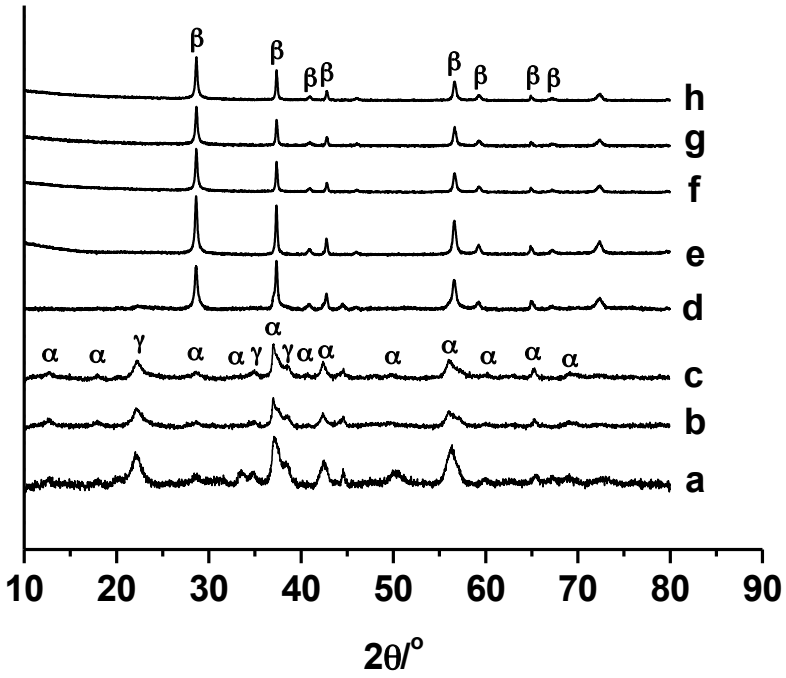

Figure 2 SEM micrographs showing the effect of crystallisation time on the MnO_2 morphology: (a) MnO_2-6h, (b) MnO_2-12h, (c) MnO_2-24h, (d) MnO_2-48h, (e) MnO_2-72h, (f) MnO_2-96h, (g) MnO_2-120h and (h) MnO_2-240h.

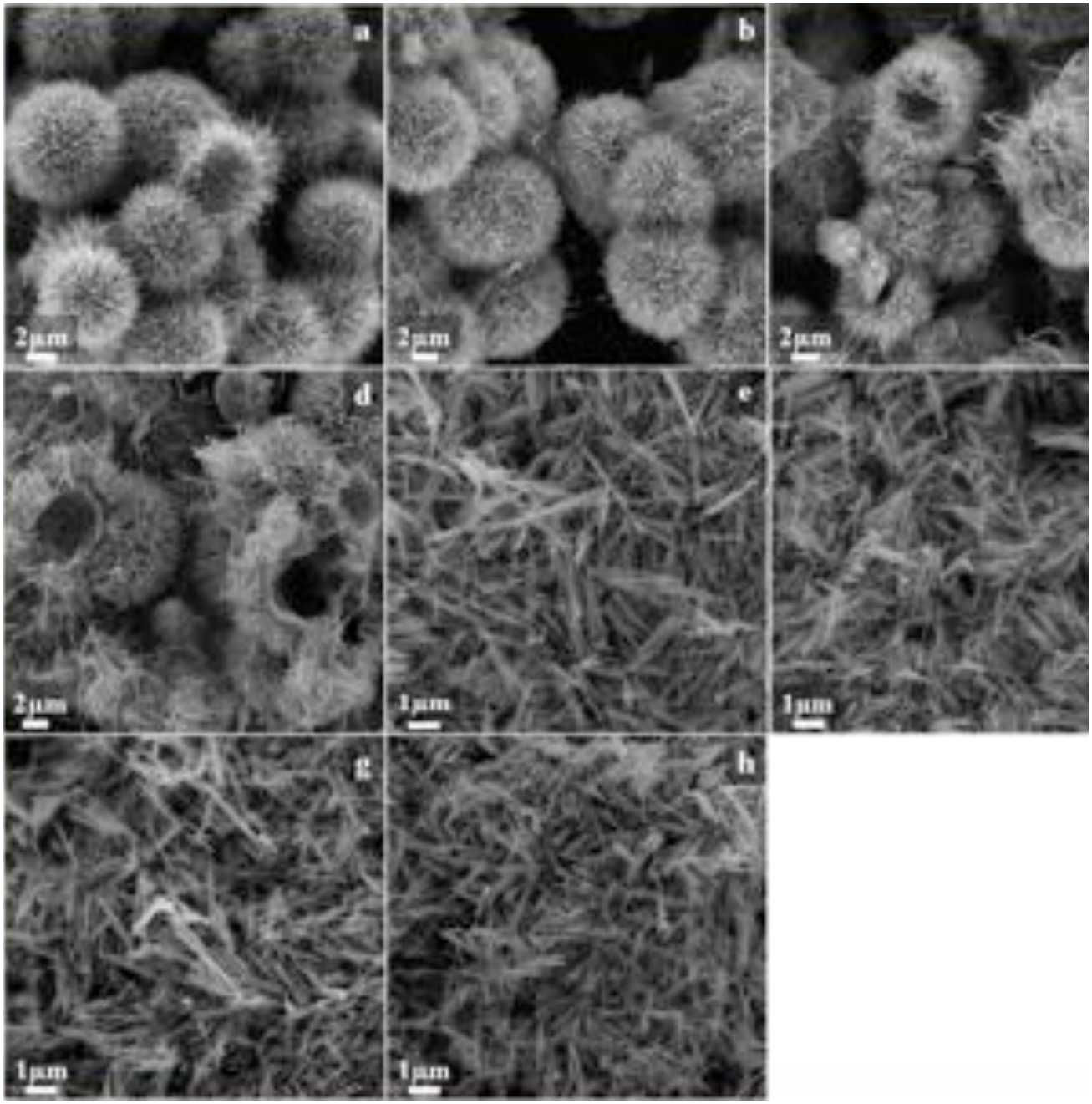

Figure 3 SEM micrographs of the Au/MnO_2 catalyst materials prepared by sol-immobilisation: (a) $1\%Au/MnO_2$-6h, (b) = $1\%Au/MnO_2$-12h, (c) $1\%Au/MnO_2$-24h, (d) $1\%Au/MnO_2$-48h, (e) $1\%Au/MnO_2$-72h, (f) $1\%Au/MnO_2$-96h, (g) $1\%Au/MnO_2$-120h, (h) $1\%Au/MnO_2$-240h.

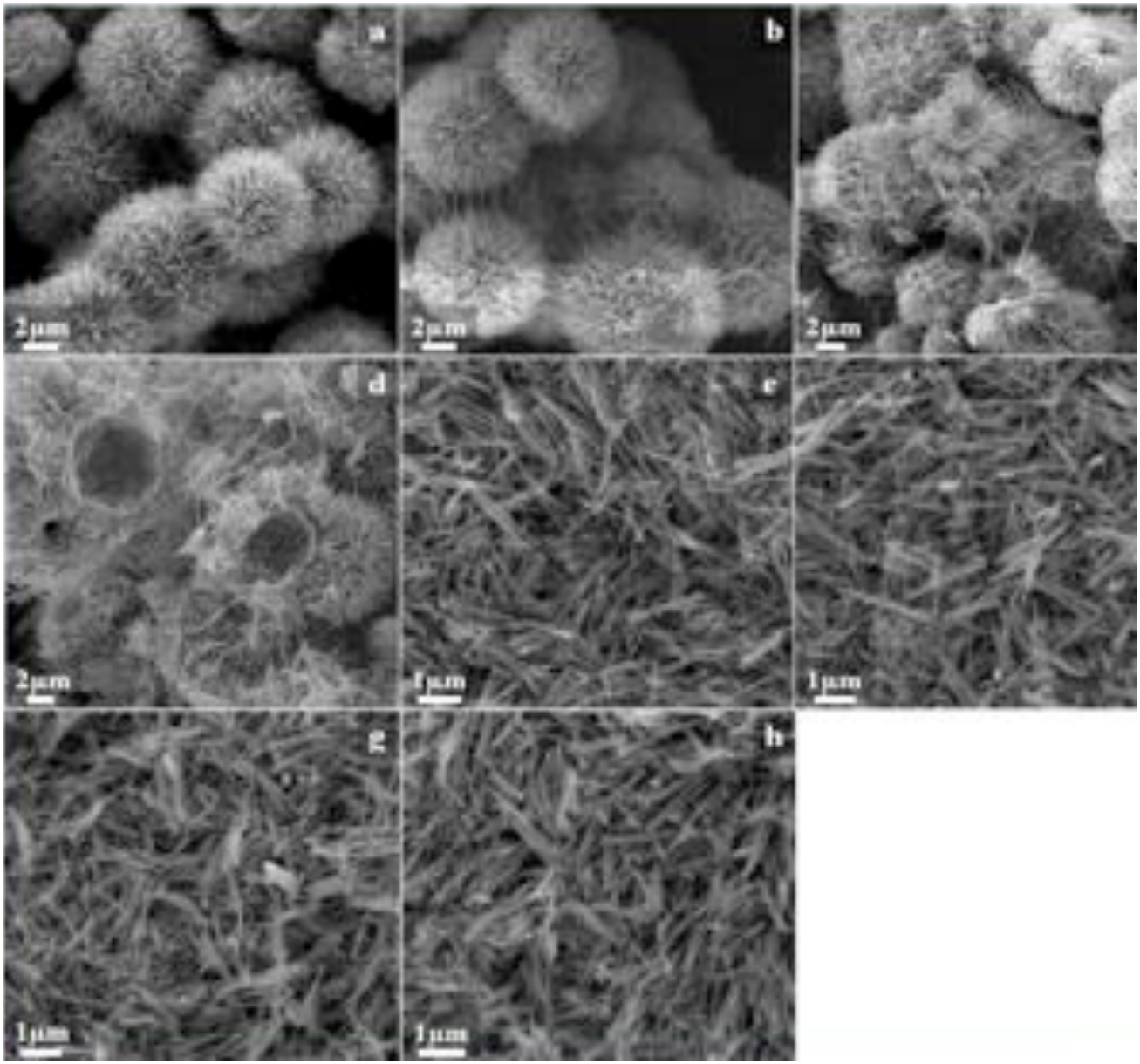

Figure 4 Bright field TEM micrographs of SI Au/MnO_2 catalysts: (a, a1) Au/MnO_2-12h, and (b, b1) Au/MnO_2-96h.

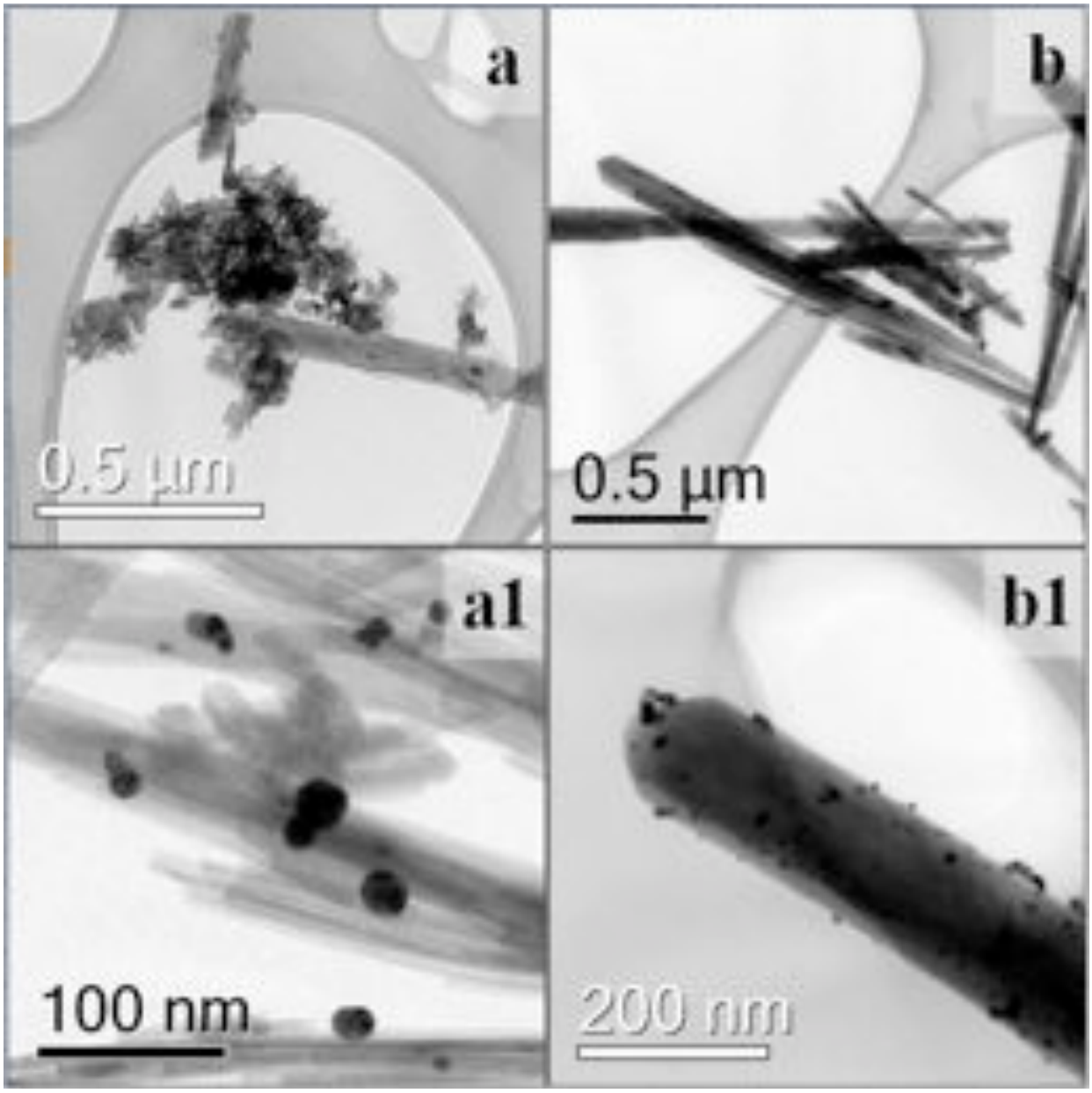

Figure 5 Raman spectroscopy analysis of: (a) SI Au/MnO_2 catalysts, and (b) reference materials.

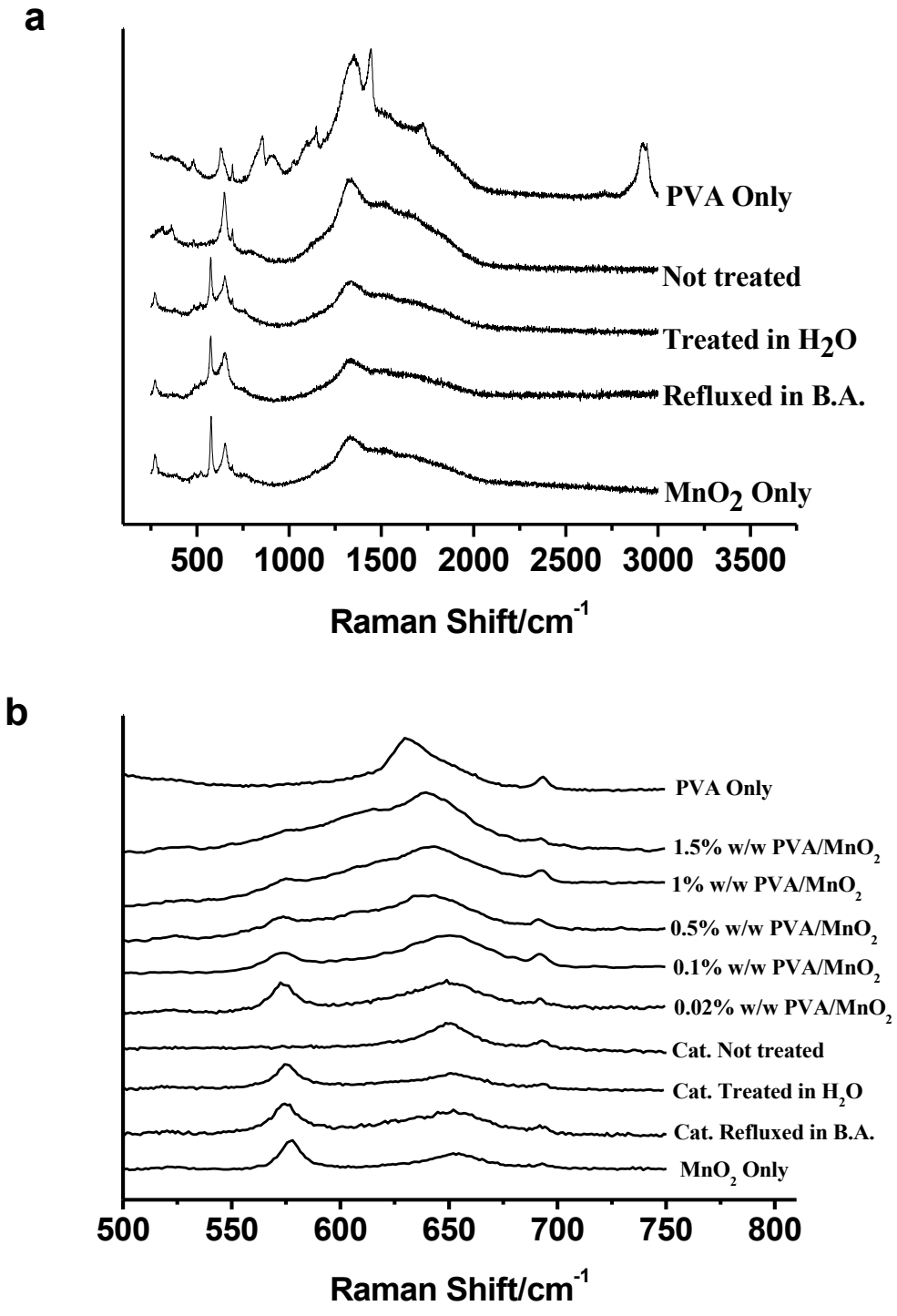

Figure 6 CO oxidation results from un-treated and water or benzyl alcohol treated 1% Au/MnO_2-12h; ■ = un-treated 1% Au/MnO_2-12h, ● = 1% Au/MnO_2-12h treated in water and ▲ = 1% Au/MnO_2-12h, ● = 1% Au/MnO_2-12h treated in benzyl alcohol.

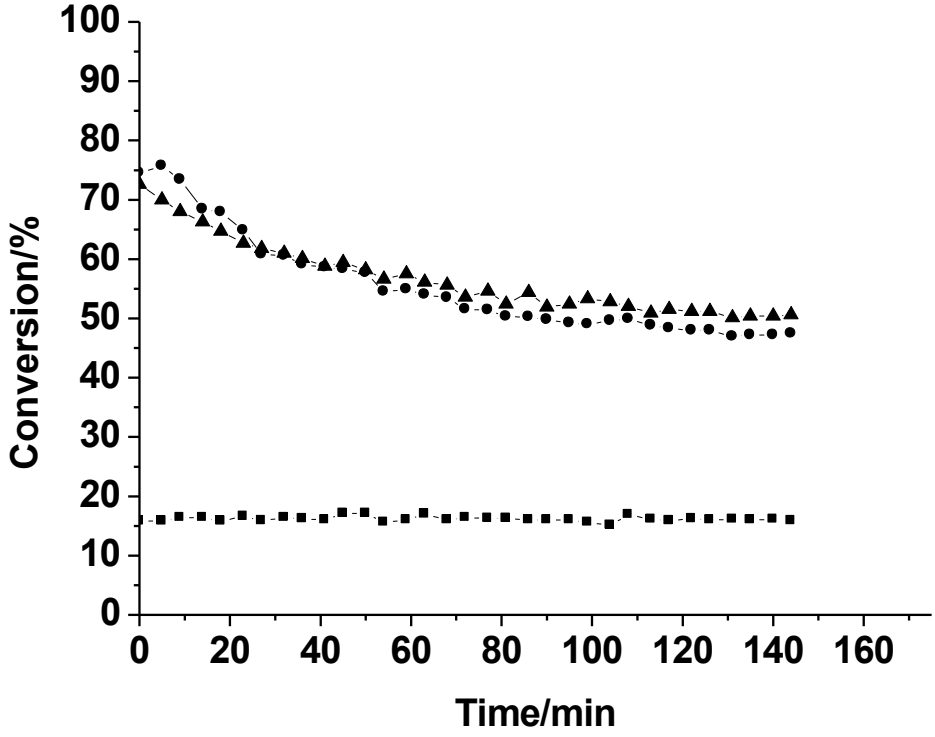

Figure 7 SEM micrographs of bare supports and catalysts prepared by sol immobilisation: (a) MnO_2-12h, (b) Au/MnO_2-12h (prior to testing), (c) Au/MnO_2-12h (post-testing) and (d) Au/MnO_2-12h (after 3rd reuse).

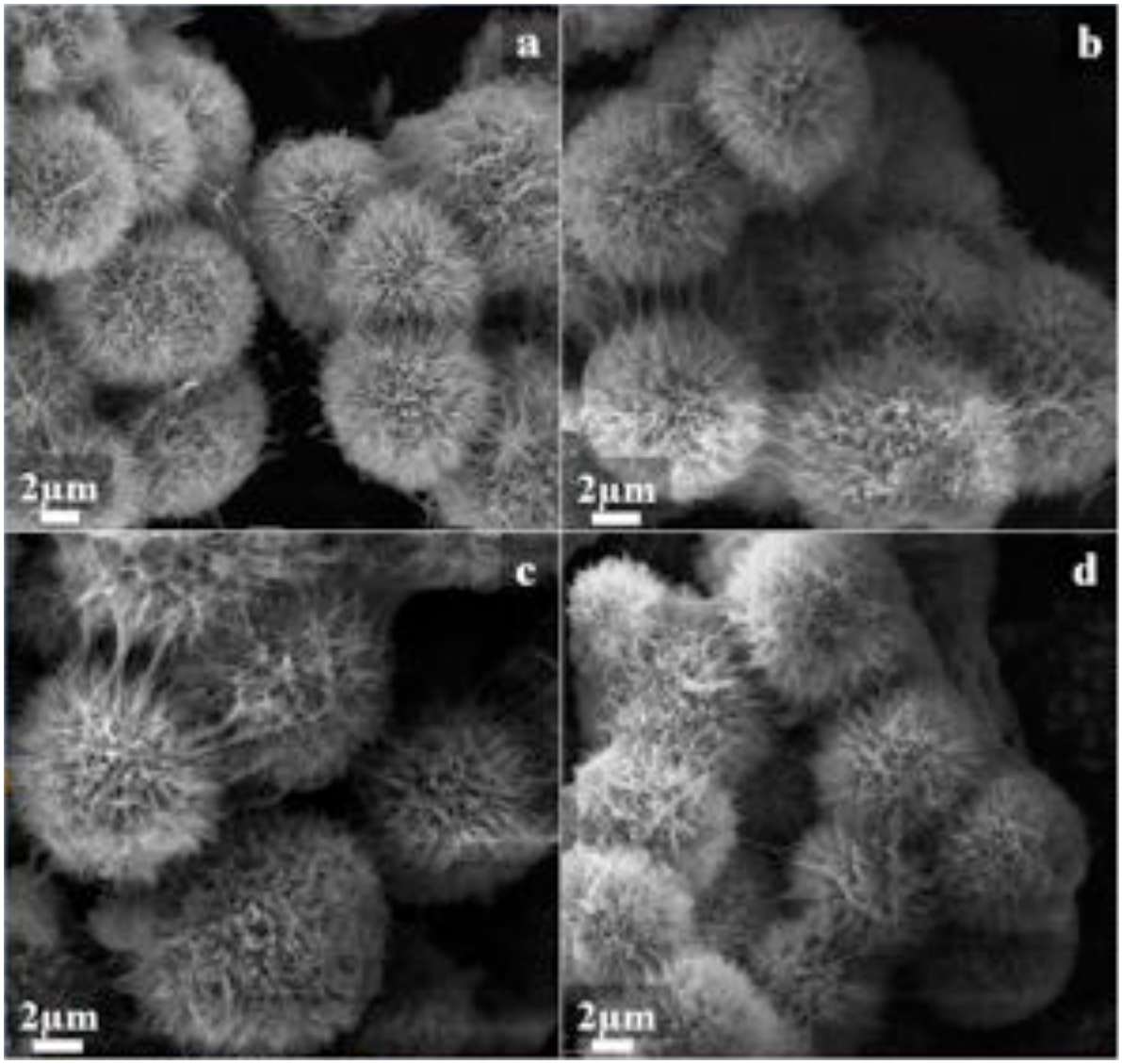

Figure 8 Oxidation of CO over 1% Au/MnO_2-12h[a] catalysts prepared by different synthesis methods: (■) WSI (STY; 4.3 $g_{CO2}/kg_{CAT}/h$), (▲) DP (STY; 4.4 $g_{CO2}/kg_{CAT}/h$), (●) SI (STY; 1.4 $g_{CO2}/kg_{CAT}/h$), (♦) IM (STY; 0.3 $g_{CO2}/kg_{CAT}/h$). Reaction conditions: CO flow rate 20 ml/min, catalyst 100 mg, 30 °C.

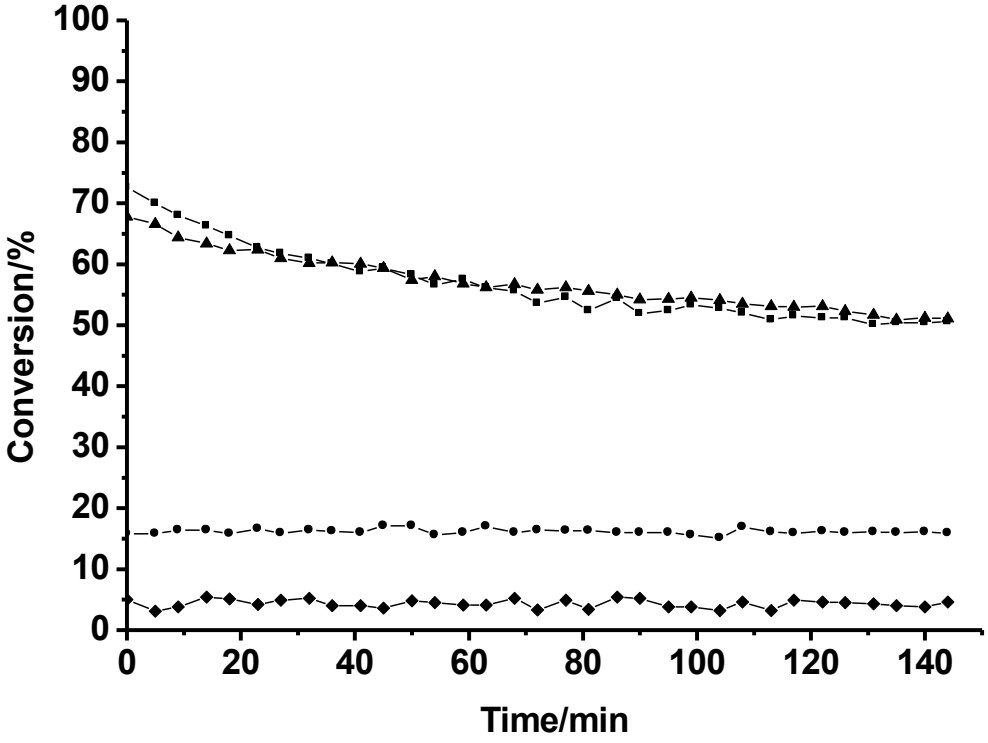

Figure 9 Representative TEM micrographs and the corresponding Au particle size distributions for: (a, a1) SI Au/MnO_2-96h, and (b, b1) DP Au/MnO_2-96h.

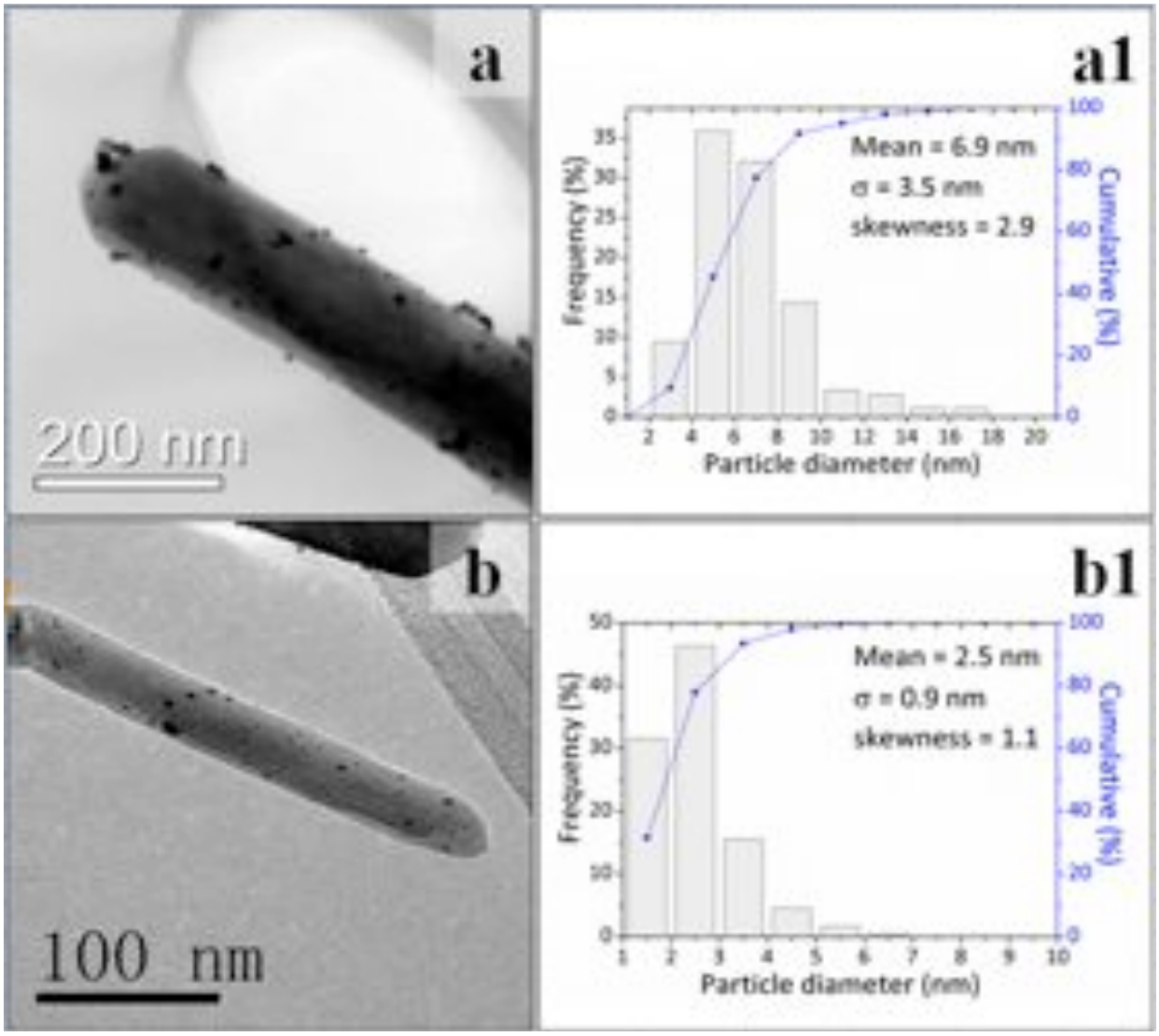

Figure 10 Representative TEM micrographs and the corresponding Au particle size distributions for: (a, a1) SI Au/MnO_2-12h, and (b, b1) DP Au/MnO_2-12h. (NB. The latter PSD (b1) was derived from measurements on electron backscatter images acquired in the SEM).

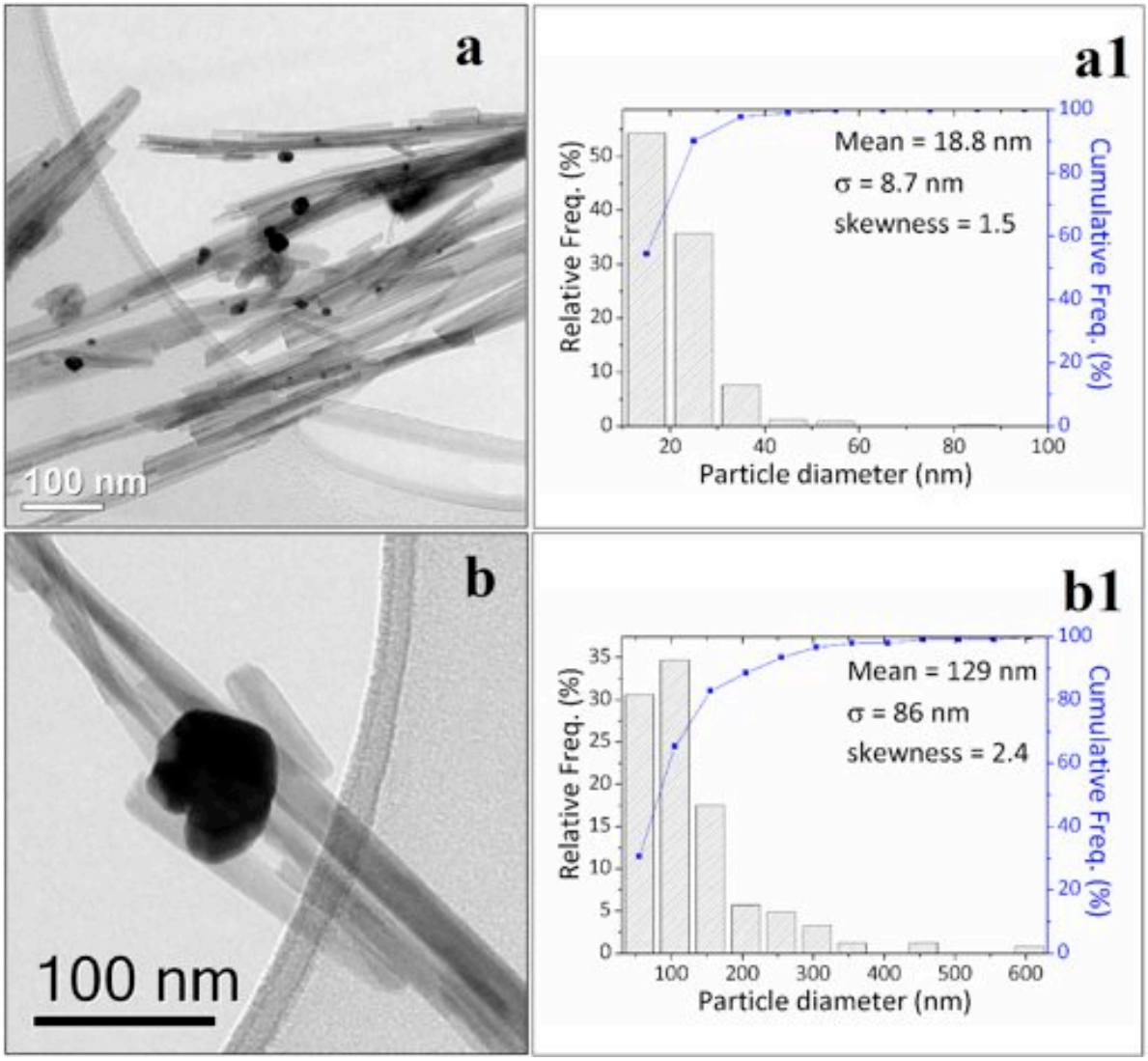

Figure 11 TPR measurements for bare support materials and Au/MnO_2 catalysts prepared using sol -immobilization: (a) MnO_2-12h, (b) SI Au/MnO_2-12h, (c) MnO_2-96h and (d) SI Au/MnO_2-96h.